

JGR Atmospheres

RESEARCH ARTICLE

10.1029/2018JD030057

Key Points:

- Modeled atmospheric ammonia concentrations is in good spatiotemporal agreement with 90 surface stations across the United States from 2007-2017
- Model underestimation is dominant in winter ($-44 \pm 58\%$ bias) across the United States, except the Pacific states ($+101 \pm 46\%$ bias)
- Model-observation correlation of seasonality is good; simulated concentrations appear more emission dominated than observations

Supporting Information:

- Supporting Information S1

Correspondence to:

A. A. Nair and F. Yu,
 aanair@albany.edu;
 fyu@albany.edu

Citation:

Nair, A. A., Yu, F., & Luo, G. (2019). Spatiotemporal variations of atmospheric ammonia concentrations over the United States: Comprehensive model-observation comparison. *Journal of Geophysical Research: Atmospheres*, 124, 6571–6582. <https://doi.org/10.1029/2018JD030057>


Received 26 NOV 2018

Accepted 21 MAR 2019

Accepted article online 28 MAR 2019

Published online 18 JUN 2019

Spatioseasonal Variations of Atmospheric Ammonia Concentrations Over the United States: Comprehensive Model-Observation Comparison

Arshad Arjunan Nair¹ , Fangqun Yu¹ , and Gan Luo¹ 

¹Atmospheric Sciences Research Center, State University of New York at Albany, Albany, NY, USA

Abstract Atmospheric ammonia plays an important role in a number of environmental issues, including new particle formation and aerosol indirect radiative forcing. Over the United States, atmospheric ammonia has seen an increasing trend due in most part to the declining SO₂ and NO_x emissions. We conduct the first comprehensive assessment of multiyear Goddard Earth Observing System (GEOS)-Chem simulated ammonia concentration ([NH₃]) over conterminous United States along with surface observations from all 90 National Atmospheric Deposition Program Ammonia Monitoring Network (AMoN) sites that have at least 2 years of continuous measurements. Model-simulated [NH₃] is along empirically expected lines with regard to temporal trends, seasonal variations, and spatial distribution. GEOS-Chem-simulated [NH₃], compared to AMoN observed values, has weighted average correlation (τ) of 0.50 ± 0.15 and mean fractional bias (*MFB*) of $-8.8 \pm 56\%$. Most sites (63 out of 90) have $-60\% < MFB < +60\%$. The deviations from observed values vary spatially and seasonally, and there is significant wintertime underestimation ($-44 \pm 58\%$) across most of conterminous United States (except the Pacific states). The largest positive deviations occur in the Pacific states ($101 \pm 46\%$) and the largest negative deviations in the Southern Plain states ($-73 \pm 39\%$) and the Mountain states ($-73 \pm 84\%$), both in the winter months. Over the Great Plains region, GEOS-Chem simulated [NH₃] shows a much stronger dependence to emissions than AMoN observed [NH₃], indicating scope for improved representation of emissions for the region. Over Southeast United States, there appears to be the strong effect of the changing emissions of SO₂ and NO_x in both modeled and observed [NH₃].

1. Introduction

Ammonia (NH₃) plays a significant role in the atmosphere due to its alkalinity and abundance. Its neutralization of acidic species resulting from SO₂ and NO_x (the acid precursor gases) that contributes to PM_{2.5} formation, as well as its effects through particulate ammonium (pNH₄⁺) on air quality and radiative forcing are important. The direct (gas phase) and indirect (through PM_{2.5}) effects of NH₃ on human health and ecosystems are well documented (Beem et al., 2010; Clark & Tilman, 2008; Ellis et al., 2013; Erisman et al., 2007; Fangmeier et al., 1994; Hautier et al., 2014). Throughout the United States, there has been an increasing trend in [NH₃] in the recent years despite relatively constant NH₃ emissions (Butler et al., 2016; Li et al., 2016; Yao & Zhang, 2016; Yu, Nair, & Luo, 2018); stringent emission control regulations have resulted in a steady decline in the concentration of acid precursor gases that reduces the participation of NH₃ in neutralization reactions in the atmosphere and permits more of it to remain in the gas phase. NH₃ has also recently received renewed attention due to its role in enhancing atmospheric new particle formation (NPF; Dunne et al., 2016; Kirkby et al., 2011; Yu, Nadykto, et al., 2018) by several hundredfold even at tens of parts per trillion by volume levels, with important implications to the number concentration of cloud condensation nuclei and aerosol indirect radiative forcing, which has the largest uncertainties in climate change projections. The high sensitivity of atmospheric NPF rates to [NH₃] (Kirkby et al., 2011; Yu, Nadykto, et al., 2018) may suggest that the uncertainty in model simulated [NH₃] may lead to additional uncertainty in aerosol indirect forcing and hence climate change projection. These factors deem it is necessary to evaluate the robustness of model predicted spatiotemporal variations of [NH₃] in the atmosphere.

Our literature review indicates that the existing model-observation comparisons of [NH₃] are limited in spatiotemporal coverage. Most of these studies focus on using the Goddard Earth Observing System (GEOS)-Chem model over the United States (Heald et al., 2012; Paulot et al., 2014; Schiferl et al., 2016; Walker

et al., 2012; Yu, Nair, & Luo, 2018; Zhang et al., 2012; Zhu et al., 2015). GEOS-Chem underestimation of $[\text{NH}_3]$ over the United States from 2006–2008 was identified to be due to excessive nitric acid formation from N_2O_5 hydrolysis in the model (Zhang et al., 2012). In contrast, negative bias in modeled nitrate over California was identified (Heald et al., 2012; Walker et al., 2012), likely due to a negative bias in NH_3 emission estimates and the effect of topography in the region causing erroneous mixed-layer heights in the model. Toward the improvement of GEOS-Chem-simulated $[\text{NH}_3]$, optimizations were made using adjoint inversion of NH_4^+ wet deposition fluxes (Paulot et al., 2014), satellite-based observational constraints (Zhu et al., 2013), or bidirectional exchange schemes (Zhu et al., 2015). Schiferl et al. (2016) examined modeled $[\text{NH}_3]$ over a 5-year period (2008–2012) over the United States with surface, aircraft, and satellite measurements. In their comparison with data from 11 National Atmospheric Deposition Program (NADP) Ammonia Monitoring Network (AMoN) sites, they generally find a high bias in Eastern United States and a low bias in Western United States. Our recent work (Yu, Nair, & Luo, 2018) examines the long-term (17 years: 2001–2016) trend of GEOS-Chem simulated $[\text{NH}_3]$ over the United States. An empirically consistent increase in $[\text{NH}_3]$ identified over the United States, with largest increase in the east, is attributable to decreasing SO_2 and NO_x emissions. Battye et al. (2016) evaluated $[\text{NH}_3]$ predictions in the NOAA National Air Quality Forecast Capability using in situ aircraft, ground-level, and satellite measurements from the DISCOVER-AQ Colorado campaign and showed the model underestimated $[\text{NH}_3]$ in Northeast Colorado by a factor of 2.7. Over other regions, there have been model evaluation using ground-based measurements for $[\text{NH}_3]$. Skjøth et al. (2004) implemented a dynamical NH_3 emission parameterization into Atmospheric Chemistry and Deposition model (a large-scale air pollution model); their model-observation comparison with monthly data from three Danish sites yielded a correlation of $r = \{0.83, 0.90, 0.93\}$ and mean square error of $\{0.59, 0.16, 0.14\} (\mu\text{gN}/\text{m}^3)^2$. At a site in Hungary, Horvath et al. (2009) showed general agreement of the European Monitoring and Evaluation Programme model with observations of increasing $[\text{NH}_3]$ from 1995–2004. Evaluation of the Danish Ammonia Modelling System model with $[\text{NH}_3]$ measurements over 21 Danish sites by Geels et al. (2012) showed model overestimation with Pearson correlation coefficients of 0.67–0.94. For six sites near Toronto, Canada, from June–November 2006, Wen et al. (2013) report $[\text{NH}_3]$ model-observation correlation of $r = 0.807$ using their modification of Stochastic Time-Inverted Lagrangian Transport-Chemistry model and biweekly observations from the Southern Ontario Ammonia Passive Sampler Survey. However, these studies showed significant deviation from a linear relationship between modeled and observed $[\text{NH}_3]$, the assumption of which is implicit in the use of these statistical evaluation parameters (discussed in section 2.3) and can obscure the identification of avenues for model improvement.

The present study is a comprehensive spatiotemporal assessment of multiyear GEOS-Chem model simulated $[\text{NH}_3]$ over the conterminous United States (CONUS) with observations from the AMoN, which was established in October 2007. Previous assessments have been limited to shorter time periods ($\ll 10$ years) and fewer locations of observational data; this study uses AMoN $[\text{NH}_3]$ data for all available surface stations and during the whole measurement periods. We also categorize the CONUS into subregions based on land use. Our focus is the spatiotemporal variation of $[\text{NH}_3]$ over the United States, with the aim of identifying model-observation discrepancies at the subregional and seasonal scales and uncovering possible avenues for their resolution such as improvements in emission inventory and land use considerations, thermodynamic partitioning schemes, and topography among others. Such a model assessment with empirical data is necessary for improved modeling of ammonia concentrations over the United States, considering its expected increasing concentration and its role in various atmospheric chemical processes, such as $\text{PM}_{2.5}$ formation and atmospheric NPF, leading to increased aerosol loading.

2. Data and Methods

2.1. Model and Simulation

GEOS-Chem: a global 3-D chemical transport model with the implementation of the Advanced Particle Microphysics package (Yu & Luo, 2009) is employed in the present study. GEOS-Chem is driven by assimilated meteorological observations from the GEOS of the National Aeronautics and Space Administration (NASA) Global Modeling and Assimilation Office. Several research groups develop and use this model, which contains numerous state-of-the-art modules treating emissions (Keller et al., 2014; van Donkelaar

et al., 2008) and various chemical and aerosol processes (e.g., Bey et al., 2001; Evans & Jacob, 2005; Martin et al., 2003; Murray et al., 2012; Park et al., 2004; Pye & Seinfeld, 2010) for solving a variety of atmospheric composition research problems.

The present study uses GEOS-Chem version 10-01, where major atmospheric components are simulated with the NO_x-O_x-hydrocarbon-aerosol chemistry (Bey et al., 2001; Martin et al., 2003), thermodynamic equilibrium of inorganic aerosols is calculated using the ISORROPIA II scheme (Fountoukis & Nenes, 2007), and formation and aging of secondary organic aerosols are based on the mechanisms developed by Pye and Seinfeld (2010) and Yu (2011). The horizontal resolution of GEOS-Chem in this study is 2° × 2.5°, with 47 vertical layers (14 layers from surface to 2 km above the surface). Global Modeling and Assimilation Office Second Modern-Era Retrospective analysis for Research and Applications meteorology fields are used to drive GEOS-Chem, and simulations are carried out for 2001–2017. Biogenic emissions and biomass burning emissions are produced by Model of Emissions of Gases and Aerosols from Nature version 2.1 (Guenther et al., 2012) and Global Fire Emissions Database (Giglio et al., 2013), respectively. Over the United States, the focus of the present study, anthropogenic emissions in GEOS-Chem are based on the Environmental Protection Agency (EPA)'s National Emission Inventory (NEI) 2011 preprocessed with the EPA Sparse Matrix Operator Kernel Emissions platform (<https://www.cmascenter.org/smoke/>). Agricultural ammonia emissions in the NEI2011 inventory are also scaled to match optimized emissions from the MASAGE_NH₃ inventory (Paulot et al., 2014). Scaling factors are generated by comparing the 2005–2008 averaged MASAGE_NH₃ agricultural emissions with the NEI2011 agricultural emissions. This treatment allows the model to retain the spatial and temporal variability in NEI2011 while matching the optimized totals from MASAGE_NH₃. For multiple-year simulations presented here, Air Pollutant Emissions Trends Data from 1990 to 2017 reported by EPA (annual total emission amounts) are used to scale NEI2011 emission inventories of CO, NO, SO₂, NH₃, black carbon, organic carbon, and volatile organic compounds from year 2011 to simulation year.

2.2. In situ measurements

In situ observations for the assessment of model simulated [NH₃] are obtained from the AMoN, which provides a consistent and long-term [NH₃] record over North America from 2007. The NADP provides AMoN data (National Atmospheric Deposition Program, 2017), which are biweekly averages of surface [NH₃] obtained using Radiello® passive diffusion samplers. [NH₃] is estimated by flow injection analysis of sonically dislodged ammonium ions from the phosphoric acid sorbent of the diffusion sampler. Data from 18 of the longest operational AMoN sites shows increasing [NH₃] trends over the United States (Butler et al., 2016). There are 114 AMoN sites; however, only 90 sites meet our criteria of location in the CONUS and with at least 24 months of continuous data within the GEOS-Chem simulation period. Monthly averaged data are obtained from the biweekly data by weighted averaging based on the number of days the 2-week period has within a month. Butler et al. (2016), in their study, grouped the 18 AMoN sites they considered into spatially proximal subregions. Land use, which is important for emission-dependent [NH₃], forms the basis of grouping these selected AMoN sites in the present study. Roughly, Eastern United States is dominated by forest land, Central United States by agricultural land, and Western United States by grassland/pasture land. We expand the categorization beyond East-Central-West to account for land use; the AMoN sites are categorized into 10 subregions of CONUS: Pacific, Mountain, Northern Plains, Southern Plains, Lake States, Corn Belt, Delta States, Southeast, Appalachia, and Northeast as defined by Bigelow and Borchers (2017).

2.3. Statistical Methods

Model-observation comparisons are necessary not just for model evaluation; they contribute to identification and rectification of deficiencies in the processes within the model. In our assessment, we use statistical parameters to quantify the degree of model-observation agreement. In this work, we use the Kendall rank correlation coefficient (τ) and mean fractional bias (*MFB*) as metrics of correlation and deviation, respectively. These statistical parameters are more robust (as discussed later in this section) than the conventionally used Pearson product-moment correlation coefficient (r) and Mean Normalized Error (*MNE*; or similar parameters).

The Pearson product-moment correlation coefficient (r) is defined as

$$r = \frac{\sum_{i=1}^n (C_m[i] - \overline{C_m})(C_o[i] - \overline{C_o})}{\sqrt{\sum_{i=1}^n (C_m[i] - \overline{C_m})^2} \sqrt{\sum_{i=1}^n (C_o[i] - \overline{C_o})^2}}$$

and the *MNE* as

$$MNE = \frac{1}{n} \sum_{i=1}^n \frac{|C_m[i] - C_o[i]|}{C_o[i]}$$

where n is the sample size, C_m denotes the modeled value, and C_o denotes the observed value.

In the use of Pearson's r are the following assumptions: (1) continuous measurements with pairwise complete observations for the two samples being compared (2) absence of outliers (3) Gaussian distribution of values (4) linearity between the two distributions, with minimal and homogenous variation about the linear fit (homoscedasticity). In the use of *MNE*, it is assumed that observed values are true values and not just estimates. *MNE* can easily blow up to ∞ when observed values are very small. Further, positive bias is weighted more than negative bias. Related parameters such as Normalized Mean Bias and Error (*NMB* and *NME*) also suffer from these deficiencies.

The Kendall rank correlation coefficient (τ) is defined (Kendall, 1970) as

$$\tau = \frac{\sum_{i=2}^n \frac{\text{sgn}(C_m[i] - C_m[i-1]) \text{sgn}(C_o[i] - C_o[i-1])}{\sqrt{\binom{n}{2} - \frac{1}{2} \sum_{i=1}^n t_m[i](t_m[i]-1)} \sqrt{\binom{n}{2} - \frac{1}{2} \sum_{i=1}^n t_o[i](t_o[i]-1)}}$$

and the Mean Fractional Bias (*MFB%*) as

$$MFB\% = \frac{1}{n} \sum_{i=1}^n \frac{C_m[i] - C_o[i]}{\frac{C_m[i] + C_o[i]}{2}} \times 100\%$$

where n is the sample size, C denotes the value, t denotes the number of ties in the i th group of ties, and subscripts denote modeled (m) and observed (o) values.

Kendall's τ is a nonparametric rank correlation coefficient that is not constrained by the assumptions in the use of Pearson's r . This parameter is also intuitive and simpler to interpret due to (a) the maximum possible value of +1 indicative of complete concordance and the minimum possible value of -1 indicative of complete discordance and (b) the ratio of concordance to discordance being $(1 + \tau)/(1 - \tau)$ (Kendall, 1970; Noether, 1981). We define (arbitrarily) the following ranges for degree of correlation: (1) poor agreement ($\tau \leq 0.2$), (2) fair agreement ($0.2 < \tau \leq 0.4$), (3) moderate agreement ($0.4 < \tau \leq 0.6$), (4) good agreement ($0.6 < \tau \leq 0.8$), and (5) excellent agreement ($0.8 < \tau \leq 1.0$). *MFB* is not limited by the issues in the use of *MNE*. *MFB%* is symmetric about 0, with a range of $[-200\%, +200\%]$; we define (arbitrarily; factor of 1.86 deviation) that *MFB%* within $[-60\%, +60\%]$ indicates that GEOS-Chem performs well in reproducing observed $[\text{NH}_3]$, *MFB%* $> +60\%$ is overestimation, and *MFB%* $< -60\%$ is underestimation. While the discussion in this manuscript is with the help of τ and *MFB%*, the supporting information contains the relevant Figures S1–S3 and Tables S1 and S2 based on the r and *MNE%* parameters.

Statistical analyses are performed using the R programming language (R Core Team, 2018) and with the aid of the “Kendall” package (McLeod, 2011). Extraction of trend and seasonality from time series data is as detailed in Cleveland et al. (1990).

2.4. Model-Observation Comparison

GEOS-Chem simulations are run for 2000–2017 over the United States and monthly means of simulated $[\text{NH}_3]$ are derived. AMoN observed $[\text{NH}_3]$ are obtained as described in section 2.2. The AMoN network first started operating from 2007 and sites have different measurement periods from 2007–2017. Monthly mean AMoN $[\text{NH}_3]$ is compared with synchronous and colocated (grid box containing AMoN site) monthly mean GEOS-Chem $[\text{NH}_3]$ using the statistical techniques in section 2.3. Since the horizontal resolution of GEOS-

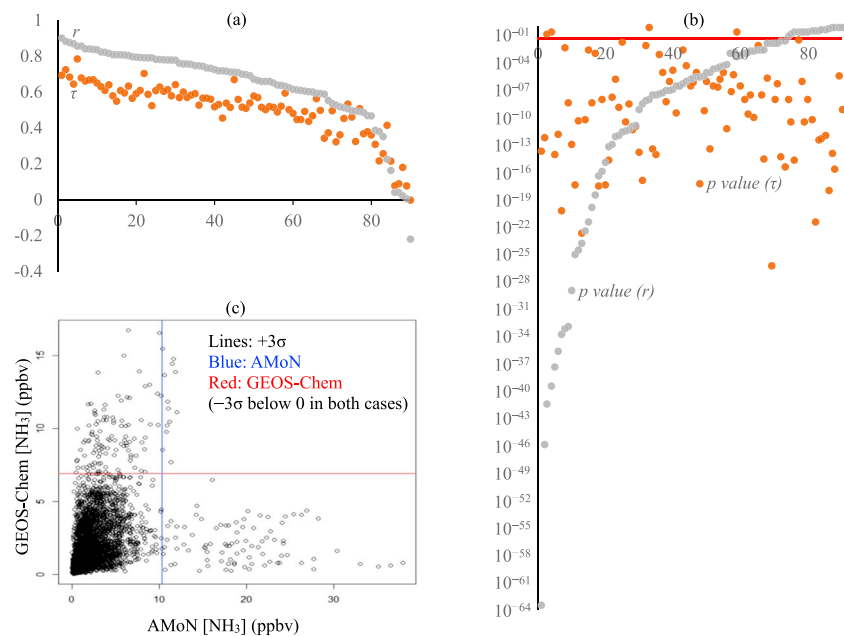


Figure 1. Comparison of GEOS-Chem simulated and AMoN observed $[NH_3]$: (a) τ versus r for each of the 90 selected AMoN sites in decreasing order of r ; (b) the associated significance (p value) for τ and r in increasing order of the p value for r (note that the axes are not the same as in panel a). Solid horizontal red line indicates p value = 0.05; and (c) scatter plot for all the pairwise complete GEOS-Chem and AMoN data for all 90 AMoN sites. Lines perpendicular to axes represent outlier limits. AMoN = Ammonia Monitoring Network.

Chem is $2^\circ \times 2.5^\circ$, the AMoN site containing model grid box may sample more emission sources and other factors affecting the spatial heterogeneity of $[NH_3]$ than the AMoN site samples locally. Table S3 shows the details of the AMoN sites by location, characteristic type based on land use, and the number of months used in the synchronous model-observation comparison. Subregional statistics are obtained by weighted averaging of the statistics of individual sites within these subregions.

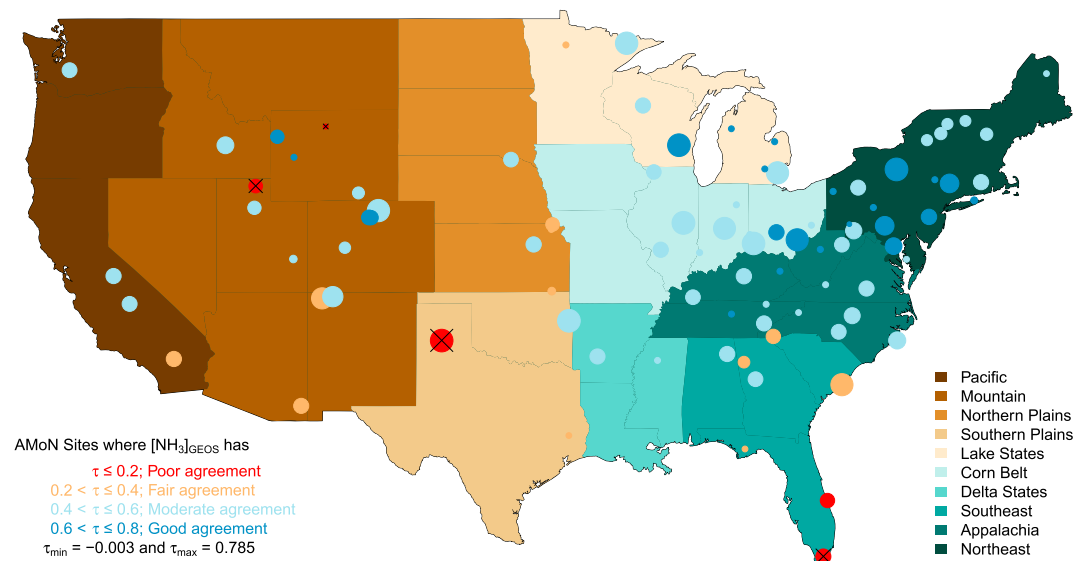


Figure 2. Location of selected Ammonia Monitoring Network (AMoN) sites across conterminous United States with at least 24 months of continuous measurements. Subregions across conterminous United States based on land use are colored as per legend (bottom right). AMoN sites locations are shown using filled circles of size relative to the months of data. Circles are colored according to the corresponding $[NH_3]_{GEOS}$ with Kendall rank correlation coefficient (τ) having the criteria detailed in the legend (bottom left). The four sites with poor model-observation agreement also have p value > 0.05, which is indicated by the X mark.

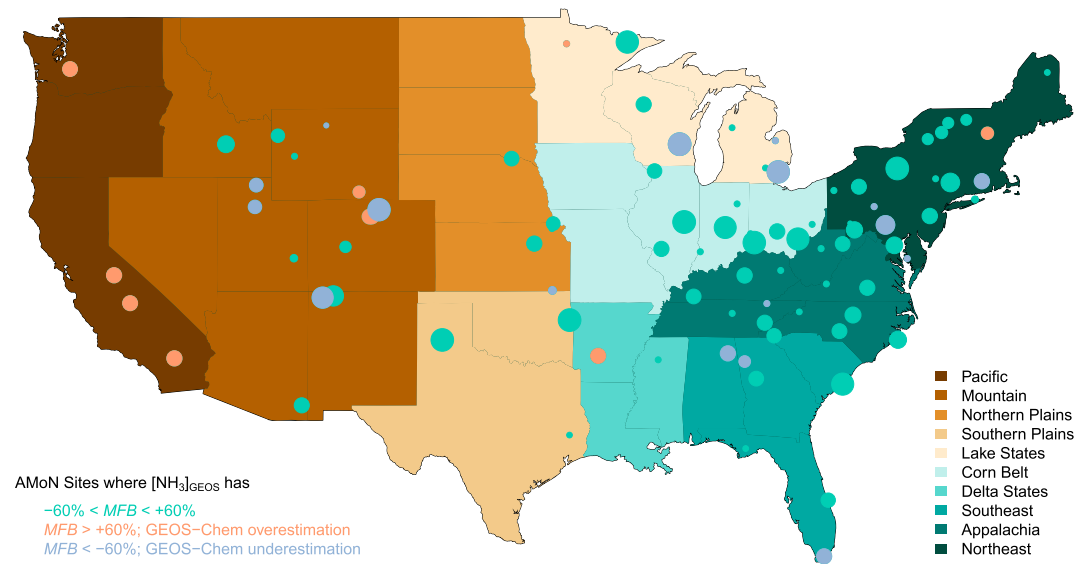


Figure 3. Location of selected Ammonia Monitoring Network (AMoN) sites across conterminous United States with at least 24 months of continuous measurements. Subregions across conterminous United States based on land use are colored as per legend (bottom right). AMoN sites locations are shown using filled circles of size relative to the months of data. Circles are colored according to the corresponding $[NH_3]_{GEOS}$ with mean fractional bias (MFB%) having the criteria detailed in the legend (bottom left).

3. Results and Discussion

3.1. Kendall's τ as a Statistical Parameter

In section 2.3, the robustness of the Kendall rank correlation coefficient (τ) over the Pearson product-moment correlation (r) is detailed. For the data used in this study, we compare the two statistical parameters to provide further justification. Figure 1a shows that the two parameters (τ and r) are correlated, making an analysis using τ comparable to that using r . That using Kendall's τ is more meaningful, at least for our study, is apparent in Figure 1b, where only 4 sites have p value > 0.05 for τ as compared to 17 sites with p value > 0.05 for r . Figure 1c for the model-observation comparison data demonstrates the invalidity of the assumptions implicit in the use of Pearson's r (detailed in section 2.3) as a statistical parameter in our study.

Table 1
Mean Fractional Bias (MFB%) for $[NH_3]_{GEOS}$ to $[NH_3]_{AMoN}$ for Each Season and Each Subregion Across CONUS

Region	Spring	Summer	Fall	Winter	All	τ	p value
	MFB%				MFB%		
Pacific (04)	91 ± 26	66 ± 31	92 ± 26	101 ± 46	87 ± 28	0.44 ± 0.14	$\ll 0.05$
Mountain (15)	-15 ± 78	-10 ± 77	-30 ± 85	-73 ± 84	-31 ± 79	0.48 ± 0.17	0.05 ± 0.17
N. Plains (05)	19 ± 40	20 ± 42	3.0 ± 43	-62 ± 36	-5.2 ± 41	0.40 ± 0.13	$\ll 0.05$
S. Plains (03)	20 ± 32	22 ± 44	-2.0 ± 51	-73 ± 39	-9.2 ± 40	0.30 ± 0.19	0.07 ± 0.08
Lake States (08)	-10 ± 56	-10 ± 58	-28 ± 74	-38 ± 70	-21 ± 63	0.58 ± 0.09	$\ll 0.05$
Corn Belt (11)	42 ± 29	5.0 ± 22	-6.0 ± 15	-28 ± 26	4.0 ± 21	0.55 ± 0.05	$\ll 0.05$
Delta States (02)	84 ± 1.5	78 ± 3.0	76 ± 3.7	4.1 ± 0.5	62 ± 1.8	0.47 ± 0.03	$\ll 0.05$
Southeast (07)	-35 ± 50	-38 ± 43	-31 ± 46	-47 ± 55	-38 ± 46	0.33 ± 0.17	0.06 ± 0.11
Appalachia (16)	6.1 ± 34	-12 ± 33	1.3 ± 30	-52 ± 38	-14 ± 26	0.52 ± 0.07	$\ll 0.05$
Northeast (19)	-0.4 ± 44	-10 ± 44	2.3 ± 38	-20 ± 46	-7.1 ± 41	0.59 ± 0.07	$\ll 0.05$
All (90)	8.4 ± 58	-2.4 ± 54	-4.6 ± 59	-37 ± 66	-8.8 ± 56	0.50 ± 0.15	0.02 ± 0.09

Note. Number of sites in each region noted in parentheses. Colored MFB% indicates GEOS-Chem overestimation (red) or GEOS-Chem underestimation (blue) at more than half of the sites in each subregion. Additionally, Kendall rank correlation coefficient (τ) for each region with associated p value. Poor correlation (for $>50\%$ sites) is indicated by red colored τ . Values are rounded averages \pm standard deviations weighted by the number of contributory observations for each site within each subregion. CONUS = conterminous United States.

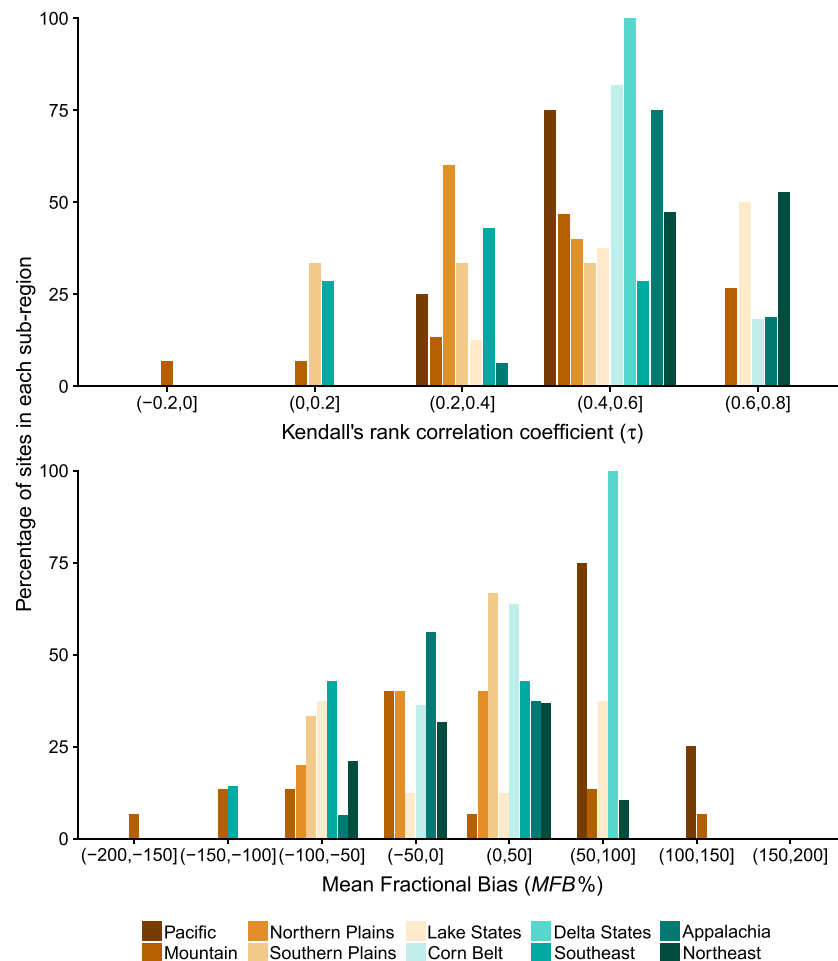


Figure 4. Bar plots for the percentage of sites in each subregion of conterminous United States in the corresponding bins for Kendall rank correlation coefficient (τ) and mean fractional bias ($MFB\%$) for $[NH_3]_{GEOS}$ compared with $[NH_3]_{AMoN}$. Subregions based on land use are colored according to the figure legend (bottom). AMoN = Ammonia Monitoring Network.

3.2. GEOS-Chem-AMoN Agreement: Correlation and Deviation

Figure 2 shows the GEOS-Chem-AMoN correlation coefficient values (τ) categorized by degree of agreement across CONUS. Kendall's τ indicates the agreement of GEOS-Chem simulated $[NH_3]$ ($[NH_3]_{GEOS}$) with AMoN observed $[NH_3]$ ($[NH_3]_{AMoN}$) for each AMoN site. The 90 AMoN sites with at least 2 year of continuous observations are located on the map and colored based on the categories of extent of model-observation correlation detailed in section 2.3. GEOS-Chem has weighted average correlation (τ) of 0.50 ± 0.15 with corresponding $[NH_3]$ values from these 90 AMoN sites. This indicates the model performs well in simulating observed $[NH_3]$. We consider $\tau > 0.4$ as strong model-observation agreement (roughly corresponding to $r > 0.5$ for the data in this study); this is the case for 85% of the AMoN sites (73 out of 86 sites with p value < 0.05).

Figure 3 shows the $MFB\%$ of $[NH_3]_{GEOS}$ compared with $[NH_3]_{AMoN}$ in the style of Figure 2; $MFB\% \approx -8.8 \pm 56\%$ over the CONUS. Most (70%: 63 out of 90) sites have $60\% < MFB < +60\%$, a range designated (section 2.3) as reasonably good performance of GEOS-Chem (Figure 3). The general tendency of GEOS-Chem is underestimation (negative MFB), which is the case over most of CONUS (Table 1).

The two statistical parameters—Kendall's τ for the correlation and $MFB\%$ for the deviation between $[NH_3]_{GEOS}$ and $[NH_3]_{AMoN}$ —indicate that the model performs well in simulating surface level $[NH_3]$ over United States.

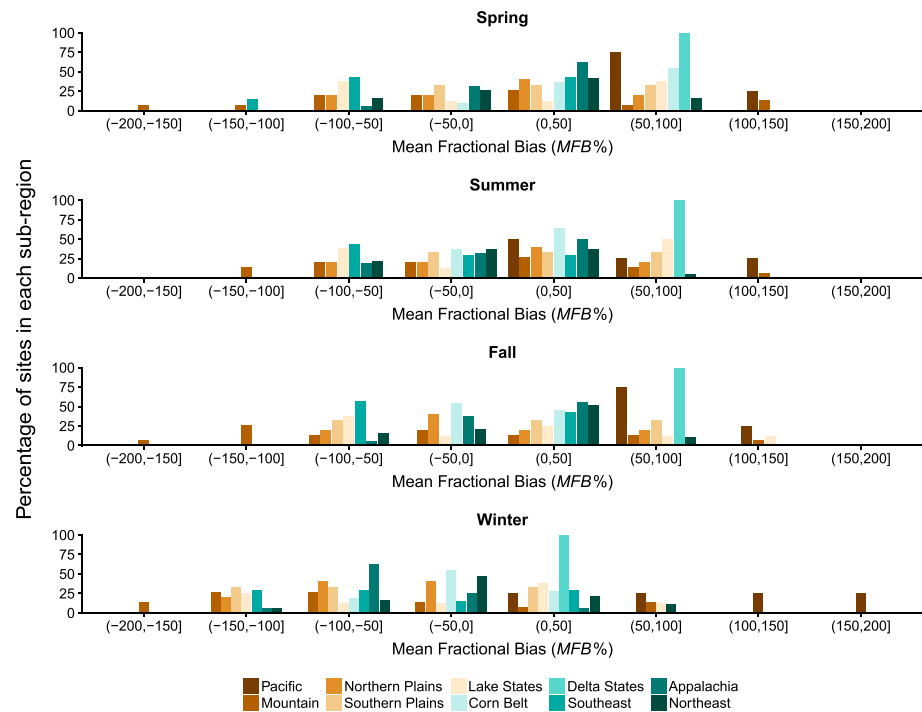


Figure 5. Bar plots for the percentage of sites in each subregion of conterminous United States in the corresponding bins for mean fractional bias (*MFB%*) for $[\text{NH}_3]_{\text{GEOS}}$ compared with $[\text{NH}_3]_{\text{AMoN}}$ for each season (from top to bottom: spring [March–May], summer [June–August], fall [September–November], and winter [December–February]). Subregions based on land use are colored according to the figure legend (bottom). AMoN = Ammonia Monitoring Network.

3.3. Spatial Variability of $[\text{NH}_3]$

$[\text{NH}_3]$ is highly emission dependent and is therefore primarily affected by land use as agriculture is the main source of gas phase ammonia emission. Most agricultural activity is concentrated in Central United States, livestock grazing is mostly across Western United States, and forestland dominates most of Eastern United States. The region-of-study is categorized on the basis detailed in section 2.2.

For a descriptive picture about the model performance, Figure 4 shows the statistical parameters (τ : correlation; *MFB*: deviation) for the agreement of $[\text{NH}_3]_{\text{GEOS}}$ to $[\text{NH}_3]_{\text{AMoN}}$ as percentage of sites in each subregion. Northeastern regions (Northeast, Lake States, Corn Belt, and Appalachia) have better correlated (τ) $[\text{NH}_3]_{\text{GEOS}}$ to AMoN values than the average across CONUS. Western regions (Southern Plains, Northern Plains, Pacific, and Mountain) have lower than average τ . Computed values for all subregions are in Table 1. This East-West contrast in GEOS-Chem performance is also reflected in the *MFB*.

3.4. Seasonal Variability in GEOS-Chem-AMoN Agreement

The seasonal weighted average deviation of $[\text{NH}_3]_{\text{GEOS}}$ compared to $[\text{NH}_3]_{\text{AMoN}}$ for each subregion is detailed in Table 1. Figure 5 provides a more detailed view of this subregional seasonal analysis with the percentage of sites within each subregion binned according to the *MFB*. At the seasonal scale, it becomes evident that there are pronounced wintertime $[\text{NH}_3]_{\text{GEOS}}$ underestimates over all subregions except the Pacific (*MFB*: $+101 \pm 46\%$) and the Delta States (*MFB*: $+4.1 \pm 0.5\%$; but a factor of ~ 20 less than other seasons). GEOS-Chem $[\text{NH}_3]$ in spring (*MFB*: $+8.4 \pm 58\%$), summer (*MFB*: $-2.4 \pm 54\%$), and fall (*MFB*: $-4.6 \pm 59\%$) do not deviate drastically from observed values, although there are variations, which are, however, within a factor of 2 deviation. There are no clear spatial patterns in the deviations for these seasons. Figure S4 shows the model-observation *MFB* variations with seasons for the 90 AMoN sites across CONUS.

3.5. Emissions and Seasonal Variability

The atmospheric concentration of ammonia is expected to be highly spatially correlated with its emission due to its relatively short atmospheric lifetime in the gas phase. In Figure 6, we examine the model

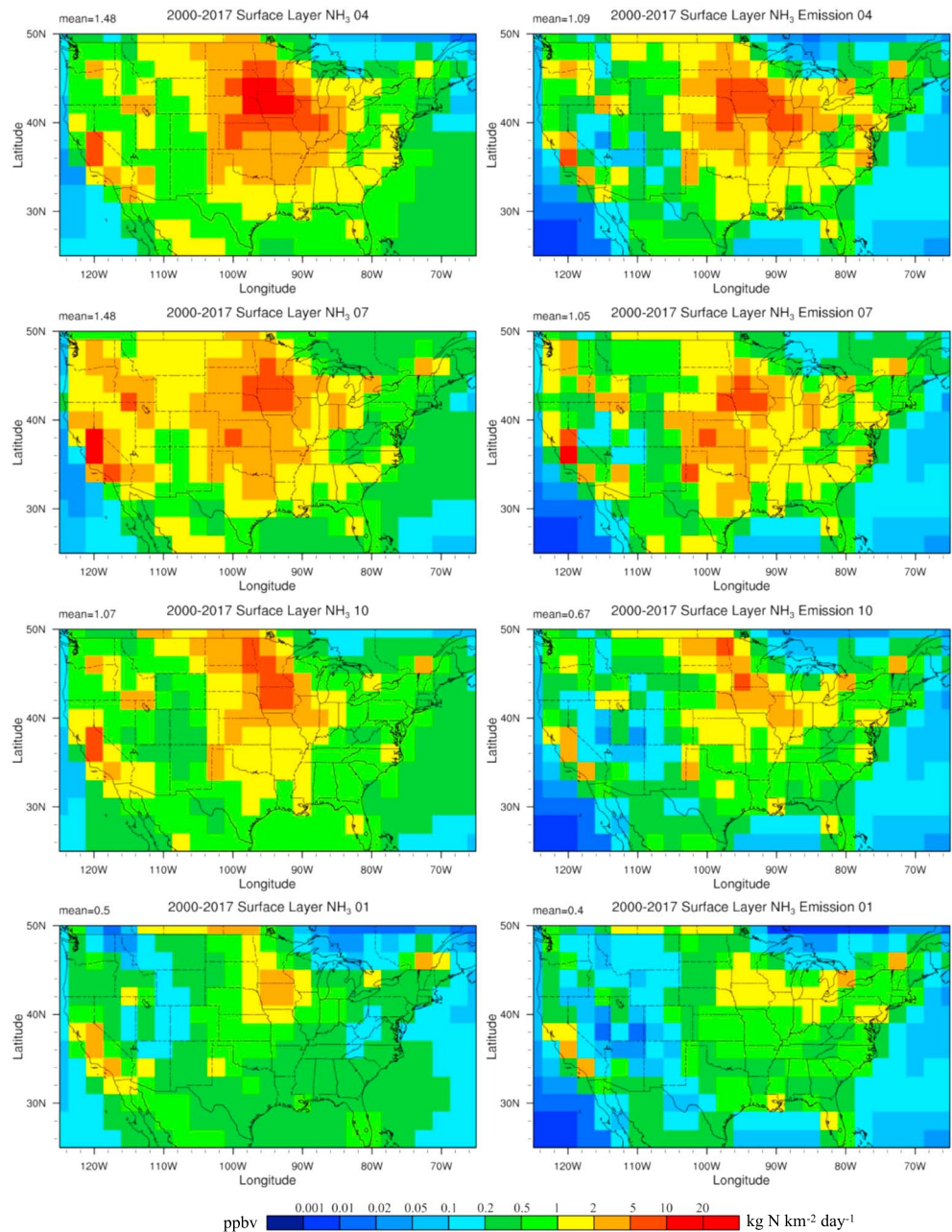


Figure 6. Seasonal spatial distribution of $[\text{NH}_3]_{\text{GEOS}}$ in parts per billion by volume (left panels) and NH_3 emission in $\text{kg N}\cdot\text{km}^{-2}\cdot\text{day}^{-1}$ from the model emission inventory (right panels) across conterminous United States. Central months are chosen to represent each season; from top to bottom: spring (April), summer (July), fall (October), and winter (January).

simulated $[\text{NH}_3]$ and NH_3 emission in the emissions inventory for each season with the spatial distribution across CONUS. There appears to be a strong effect of local emissions dictating the spatial distribution of $[\text{NH}_3]$.

Correlations (τ) of $[\text{NH}_3]_{\text{GEOS}}$ and $[\text{NH}_3]_{\text{AMON}}$ with NH_3 emission are detailed in Table 2. The correlations are expected to be strong due to the emission dependence of $[\text{NH}_3]$. $\tau_{(\text{A,E})}$ (correlation between $[\text{NH}_3]_{\text{AMON}}$ and NH_3 emission) and $\tau_{(\text{G,E})}$ (correlation between $[\text{NH}_3]_{\text{GEOS}}$ and NH_3 emission) indicate if emission is the main factor modulating respective values of $[\text{NH}_3]$. Rather than examining these correlations in isolation, a combined analysis can reveal if the emission inventory in the model is representative of real emissions

Table 2

Kendall Rank Correlation Coefficient (τ) for Comparative GEOS-Chem(G)-AMoN(A)-Emission(E) Statistics for Time Series (the Sequence of Data Coincident With at Least 24 Months of Continuous AMoN Data for Each Site) and Estimated Seasonality (Seasonal Decomposition of This Time Series by Locally Estimated Scatterplot Smoothing) for Each Region Weighted by the Number of Contributory Observations for Each Site Within Each Subregion

τ	(G,E)	(A,E)	(G,A)
<i>Time series</i>			
Pacific (04)	0.55 ± 0.19	0.65 ± 0.07	0.44 ± 0.14
Mountain (15)	0.78 ± 0.06	0.51 ± 0.18	0.48 ± 0.17
N. Plains (05)	0.54 ± 0.06	0.26 ± 0.17	0.39 ± 0.13
S. Plains (03)	0.66 ± 0.03	0.25 ± 0.14	0.30 ± 0.19
Lake States (08)	0.57 ± 0.15	0.55 ± 0.10	0.58 ± 0.09
Corn Belt (11)	0.51 ± 0.06	0.54 ± 0.12	0.56 ± 0.05
Delta States (02)	0.50 ± 0.03	0.34 ± 0.09	0.47 ± 0.03
Southeast (07)	0.34 ± 0.24	0.30 ± 0.14	0.33 ± 0.17
Appalachia (16)	0.57 ± 0.07	0.51 ± 0.09	0.51 ± 0.07
Northeast (19)	0.62 ± 0.05	0.63 ± 0.08	0.59 ± 0.07
All (90)	0.59 ± 0.16	0.50 ± 0.17	0.50 ± 0.15
<i>Estimated seasonality</i>			
Pacific (04)	0.63 ± 0.17	0.84 ± 0.06	0.62 ± 0.12
Mountain (15)	0.83 ± 0.05	0.71 ± 0.28	0.64 ± 0.26
N. Plains (05)	0.61 ± 0.08	0.37 ± 0.28	0.60 ± 0.20
S. Plains (03)	0.81 ± 0.04	0.43 ± 0.30	0.46 ± 0.34
Lake States (08)	0.65 ± 0.20	0.71 ± 0.10	0.68 ± 0.12
Corn Belt (11)	0.55 ± 0.05	0.74 ± 0.14	0.63 ± 0.08
Delta States (02)	0.59 ± 0.09	0.50 ± 0.02	0.75 ± 0.06
Southeast (07)	0.47 ± 0.30	0.61 ± 0.31	0.42 ± 0.28
Appalachia (16)	0.70 ± 0.09	0.73 ± 0.14	0.60 ± 0.09
Northeast (19)	0.74 ± 0.07	0.76 ± 0.10	0.73 ± 0.06
All (90)	0.68 ± 0.17	0.69 ± 0.22	0.63 ± 0.20

Note. Error limits correspond to $\pm 1\sigma$. AMoN = Ammonia Monitoring Network.

and if simulated concentrations are accurate. $\tau_{(A,E)}$ is low (< 0.4 and $\ll \tau_{(G,E)}$) for sites in the Northern Plains, Southern Plains, and Delta States. We avoid discussing the Delta states due to only two sites being present in this subregion. For the estimated seasonality, $\tau_{(A,E)(S)}$ is low in the Great Plains region (Northern and Southern Plains) and about 2 times lower than $\tau_{(G,E)(S)}$. The magnitude and seasonal variation of $[\text{NH}_3]_{\text{GEOS}}$ is more strongly correlated with NH_3 emissions than $[\text{NH}_3]_{\text{AMoN}}$. This could indicate an issue with the representation of emission in the emission inventory for the Great Plains region. $\tau_{(A,E)}$ is low (< 0.4) but $\approx \tau_{(G,E)}$ for sites in the Southeast, $\tau_{(A,E)(S)}$ for the estimated seasonality is good (0.61 ± 0.31), but $\tau_{(G,A)}$ and $\tau_{(G,A)(S)}$ are low. Although NH_3 emission controls the seasonal variation of $[\text{NH}_3]$ strongly in the Southeast, some process other than emission could have a stronger effect in determining the magnitude/trend of $[\text{NH}_3]$. In Yu, Nair, and Luo (2018), this region is identified as one of the U.S. regions with the highest increasing long-term trend of $[\text{NH}_3]$ and the largest decline in SO_2 and NO_x emissions (see also Figure S5). The high acidity of fine particles in the Southeast as well as low participation of NO_3 in the aerosol could also be responsible for this observation (Guo et al., 2018). This aspect deems further investigation, which is beyond the scope of the present study. The final column in Table 2 details the correlation between $[\text{NH}_3]_{\text{GEOS}}$ and $[\text{NH}_3]_{\text{AMoN}}$, which has been previously discussed in section 3.4. In addition to the information already in Table 1, we examine these correlations in seasonality; $\tau_{(G,A)(S)}$ are > 0.6 for all regions, except the Southern Plains and the Southeast, problematic subregions identified above. We refrain from interpreting the correlations of the estimated trends from the time series due to emissions not having a strong temporal trend.

4. Summary

We comprehensively assess multiyear (18 years: 2000–2017) surface layer GEOS-Chem simulated $[\text{NH}_3]$ over CONUS in the present study. The

NADP AMoN provides biweekly averaged surface $[\text{NH}_3]$ over CONUS. We use these empirical values for 90 sites that have at least 2 years of continuous surface measurements of $[\text{NH}_3]$ to assess model performance during the whole periods that measurements are available. GEOS-Chem simulated $[\text{NH}_3]$ reflects empirical values from the AMoN. GEOS-Chem simulated $[\text{NH}_3]$ values ($\tau \approx 0.50 \pm 0.15$; 70% of sites have $60\% < \text{MFB} < +60\%$), seasonality ($\tau \approx 0.63 \pm 0.20$), and spatial distribution are along empirically expected lines. Apart from the good correlation, deviations are low ($\text{MFB} \approx -8.8 \pm 56\%$) and within $\pm 60\%$. There are seasonal and spatial variations in the degree of agreement; most notably wintertime underestimation is significant ($\text{MFB}\% \approx -37 \pm 66\%$) across most subregions of CONUS. The seasonality of $[\text{NH}_3]$, unlike the long-term trend (Yu, Nair, & Luo, 2018), still shows strong dependence on the emission of NH_3 .

A caveat to be noted is that GEOS-Chem simulated $[\text{NH}_3]$ is for a $2^\circ \times 2.5^\circ$ grid box in which an AMoN site is located. The value may not necessarily reflect measured AMoN values due to the high spatial variability of $[\text{NH}_3]$. The main confounding factor is the location of NH_3 emission sources near the AMoN sites within the purview of the colocated model grid box. Typically, these sites are located away from emission sources for the measurement of background $[\text{NH}_3]$, which may, in itself, appear as model overestimation. However, some sites are located close to emission sources or where topography exacerbates $[\text{NH}_3]$, which may appear to show model underestimation. The location of AMoN sites is not spatially uniform, with variability in the number of sites in each subregion. Further, the number of observations is not the same, with sites having different operational periods and with some gaps in the measurement. We reduce the effects of these factors by selecting sites with at least 24 months of continuous data for meaningful seasonal analysis and ensure that values computed for each subregion are weighted by the number of contributory observations from each site within these subregions. Additionally, AMoN-observed $[\text{NH}_3]$ need not be true $[\text{NH}_3]$. This is due to

several factors, including (1) the 2-week (occasionally variable) averaging time of measurements, (2) offline human handling and analysis of collected samples, and (3) consistent low bias of the AMoN network (Puchalski et al., 2015). It is recommended that AMoN be expanded in its spatial distribution and heterogeneity with respect to emission source locations for a better understanding of the spatial gradients in $[\text{NH}_3]$ in the vicinity of these locations. There is scope for improved simulation of $[\text{NH}_3]$ through improved representation of emission within the model, especially over the U.S. Great Plains region. Improved emission inventories will be a consequence of integrated surface and satellite measurements at higher spatial and temporal resolution. Our analysis indicates that GEOS-Chem simulated $[\text{NH}_3]$ is more strongly dependent on emission than AMoN observed $[\text{NH}_3]$. Some process related to the changing acid precursor gas emission, or low aerosol NH_4NO_3 , or high acidity of fine particles, or a combination of these factors may be responsible for the model-observation disagreement over Southeast United States. Further study using models with higher spatial resolution is needed to assess how much the difference between the modeled and observed $[\text{NH}_3]$ shown in the present study is due to coarse spatial resolution. On the other hand, the performance of models in capturing diurnal variations of $[\text{NH}_3]$ remains to be evaluated, especially regarding the role of ammonia in NPF that generally occurs in the morning hours.

Acknowledgments

This study was supported by NASA under grant NNX13AK20G, NSF under grant AGS-1550816, and NYSERDA under contract 100416. Ammonia Monitoring Network (AMoN) data are available from National Atmospheric Deposition Program (NRSP-3), 2017, NADP Program Office, Illinois State Water Survey, University of Illinois, Champaign, IL 61820 (<http://nadp.slh.wisc.edu/amon/>). The GEOS-Chem model is a freely accessible community-driven model (<http://acmg.seas.harvard.edu/geos/>) managed by the GEOS-Chem Support Team at Harvard University and Dalhousie University with support from NASA's Earth Science Division, Natural Sciences and Engineering Research Council of Canada (NSERC), and Nanjing University of Information Sciences and Technology (NUIST). The work described in this paper is based on GEOS-Chem version 10-01. Figures in this paper were generated using R: a free statistical computing and graphics software available at <https://www.R-project.org/> and NCAR Command Language (NCL) available at <https://www.ncl.ucar.edu/> website.

References

- Battye, W. H., Bray, C. D., Aneja, V. P., Tong, D., Lee, P., & Tang, Y. (2016). Evaluating ammonia (NH_3) predictions in the NOAA National Air Quality Forecast Capability (NAQFC) using in situ aircraft, ground-level, and satellite measurements from the DISCOVER-AQ Colorado campaign. *Atmospheric Environment*, *140*, 342–351. <https://doi.org/10.1016/j.atmosenv.2016.06.021>
- Beem, K. B., Raja, S., Schwandner, F. M., Taylor, C., Lee, T., Sullivan, A. P., et al. (2010). Deposition of reactive nitrogen during the Rocky Mountain Airborne Nitrogen and Sulfur (RoMANS) study. *Environmental Pollution*, *158*(3), 862–872. <https://doi.org/10.1016/j.envpol.2009.09.023>
- Bey, I., Jacob, D. J., Yantosca, R. M., Logan, J. A., Field, B. D., Fiore, A. M., et al. (2001). Global modeling of tropospheric chemistry with assimilated meteorology: Model description and evaluation. *Journal of Geophysical Research*, *106*(D19), 23,073–23,095. <https://doi.org/10.1029/2001jd000807>
- Bigelow, D. P., & Borchers, A. (2017). Major Uses of Land in the United States, 2012. EIB-178, United States, Department of Agriculture, Economic Research Service.
- Butler, T., Vermeylen, F., Lehmann, C. M., Likens, G. E., & Puchalski, M. (2016). Increasing ammonia concentration trends in large regions of the USA derived from the NADP/AMoN network. *Atmospheric Environment*, *146*, 132–140. <https://doi.org/10.1016/j.atmosenv.2016.06.033>
- Clark, C. M., & Tilman, D. (2008). Loss of plant species after chronic low-level nitrogen deposition to prairie grasslands. *Nature*, *451*(7179), 712–715. <https://doi.org/10.1038/nature06503>
- Cleveland, R. B., Cleveland, W. S., McRae, J. E., & Terpenning, I. (1990). STL: A seasonal-trend decomposition. *Journal of Official Statistics*, *6*(1), 3–73.
- R Core Team. (2018). R: A language and environment for statistical computing [Computer software manual]. Vienna, Austria. Retrieved from <https://www.R-project.org/>
- van Donkelaar, A., Martin, R. V., Leaitch, W. R., Macdonald, A. M., Walker, T. W., Streets, D. G., et al. (2008). Analysis of aircraft and satellite measurements from the Intercontinental Chemical Transport Experiment (INTEX-B) to quantify long-range transport of East Asian sulfur to Canada. *Atmospheric Chemistry and Physics*, *8*(11), 2999–3014. <https://doi.org/10.5194/acp-8-2999-2008>
- Dunne, E. M., Gordon, H., Kurten, A., Almeida, J., Duplissy, J., Williamson, C., et al. (2016). Global atmospheric particle formation from CERN CLOUD measurements. *Science*, *354*(6316), 1119–1124. <https://doi.org/10.1126/science.aaf2649>
- Ellis, R. A., Jacob, D. J., Sulprizio, M. P., Zhang, L., Holmes, C. D., Schichtel, B. A., et al. (2013). Present and future nitrogen deposition to national parks in the United States: Critical load exceedances. *Atmospheric Chemistry and Physics*, *13*(17), 9083–9095. <https://doi.org/10.5194/acp-13-9083-2013>
- Erisman, J. W., Bleeker, A., Galloway, J., & Sutton, M. S. (2007). Reduced nitrogen in ecology and the environment. *Environmental Pollution*, *150*(1), 140–149. <https://doi.org/10.1016/j.envpol.2007.06.033>
- Evans, M. J., & Jacob, D. J. (2005). Impact of new laboratory studies of N_2O_5 hydrolysis on global model budgets of tropospheric nitrogen oxides, ozone, and OH. *Geophysical Research Letters*, *32*, L09813. <https://doi.org/10.1029/2005GL022469>
- Fangmeier, A., Hadwiger-Fangmeier, A., Van der Eerden, L., & Jäger, H.-J. (1994). Effects of atmospheric ammonia on vegetation—A review. *Environmental Pollution*, *86*(1), 43–82. [https://doi.org/10.1016/0269-7491\(94\)90008-6](https://doi.org/10.1016/0269-7491(94)90008-6)
- Fountoukis, C., & Nenes, A. (2007). ISORROPIA II: a computationally efficient thermodynamic equilibrium model for $\text{K}^+ - \text{Ca}^{2+} - \text{Mg}^{2+} - \text{NH}_4^+ - \text{Na}^+ - \text{SO}_4^{2-} - \text{NO}_3^- - \text{Cl}^- - \text{H}_2\text{O}$ aerosols. *Atmospheric Chemistry and Physics*, *7*(17), 4639–4659. <https://doi.org/10.5194/acp-7-4639-2007>
- Geels, C., Andersen, H. V., Ambelas Skjøth, C., Christensen, J. H., Ellermann, T., Lofström, P., et al. (2012). Improved modelling of atmospheric ammonia over Denmark using the coupled modelling system DAMOS. *Biogeosciences*, *9*(7), 2625–2647. <https://doi.org/10.5194/bg-9-2625-2012>
- Giglio, L., Randerson, J. T., & van der Werf, G. R. (2013). Analysis of daily, monthly, and annual burned area using the fourth-generation global fire emissions database (GFED4). *Journal of Geophysical Research: Biogeosciences*, *118*, 317–328. <https://doi.org/10.1002/jgrg.20042>
- Guenther, A. B., Jiang, X., Heald, C. L., Sakulyanontvittaya, T., Duhl, T., Emmons, L. K., & Wang, X. (2012). The model of emissions of gases and aerosols from nature version 2.1 (MEGAN2.1): An extended and updated framework for modeling biogenic emissions. *Geoscientific Model Development*, *5*(6), 1471–1492. <https://doi.org/10.5194/gmd-5-1471-2012>
- Guo, H., Otjes, R., Schlag, P., Kiendler-Scharr, A., Nenes, A., & Weber, R. J. (2018). Effectiveness of ammonia reduction on control of fine particle nitrate. *Atmospheric Chemistry and Physics*, *18*(16), 12,241–12,256. <https://doi.org/10.5194/acp-18-12241-2018>

- Hautier, Y., Seabloom, E. W., Borer, E. T., Adler, P. B., Harpole, W. S., Hillebrand, H., et al. (2014). Eutrophication weakens stabilizing effects of diversity in natural grasslands. *Nature*, *508*(7497), 521–525. <https://doi.org/10.1038/nature13014>
- Heald, C. L., Collett, J. L. Jr., Lee, T., Benedict, K. B., Schwandner, F. M., Li, Y., et al. (2012). Atmospheric ammonia and particulate inorganic nitrogen over the United States. *Atmospheric Chemistry and Physics*, *12*(21), 10,295–10,312. <https://doi.org/10.5194/acp-12-10295-2012>
- Horvath, L., Fagerli, H., & Sutton, M. A. (2009). Long-term record (1981–2005) of ammonia and ammonium concentrations at K-Puszta Hungary and the effect of sulphur dioxide emission change on measured and modelled concentrations. In M. A. Sutton, S. Reis, & S. M. Baker (Eds.), *Atmospheric Ammonia*, (pp. 181–185). Dordrecht: Springer. https://doi.org/10.1007/978-1-4020-9121-6_12
- Keller, C. A., Long, M. S., Yantosca, R. M., Da Silva, A. M., Pawson, S., & Jacob, D. J. (2014). HEMCO v1.0: a versatile, ESMF-compliant component for calculating emissions in atmospheric models. *Geoscientific Model Development*, *7*(4), 1409–1417. <https://doi.org/10.5194/gmd-7-1409-2014>
- Kendall, M. (1970). *Rank correlation methods*. London: Griffin.
- Kirkby, J., Curtius, J., Almeida, J., Dunne, E., Duplissy, J., Ehrhart, S., et al. (2011). Role of sulphuric acid, ammonia and galactic cosmic rays in atmospheric aerosol nucleation. *Nature*, *476*(7361), 429–433. <https://doi.org/10.1038/nature10343>
- Li, Y., Schichtel, B. A., Walker, J. T., Schwede, D. B., Chen, X., Lehmann, C. M. B., et al. (2016). Increasing importance of deposition of reduced nitrogen in the United States. *Proceedings of the National Academy of Sciences*, *113*(21), 5874–5879. <https://doi.org/10.1073/pnas.1525736113>
- Martin, R. V., Jacob, D. J., Yantosca, R. M., Chin, M., & Ginoux, P. (2003). Global and regional decreases in tropospheric oxidants from photochemical effects of aerosols. *Journal of Geophysical Research*, *108*, 4097. <https://doi.org/10.1029/2002JF002622>
- McLeod, A. I. (2011). Kendall: Kendall rank correlation and Mann-Kendall trend test. R package version 2.2. Retrieved from <https://CRAN.R-project.org/package=Kendall> (R package version 2.2)
- Murray, L. T., Jacob, D. J., Logan, J. A., Hudman, R. C., & Koshak, W. J. (2012). Optimized regional and interannual variability of lightning in a global chemical transport model constrained by LIS/OTD satellite data. *Journal of Geophysical Research*, *117*, D20307. <https://doi.org/10.1029/2012JD017934>
- National Atmospheric Deposition Program. (2017). Ammonia Monitoring Network (AMoN), National Atmospheric Deposition Program (NADP-3). <http://nadp.sws.uiuc.edu/AMoN/>. NADP Program Office, Illinois State Water Survey, University of Illinois, Champaign, IL 61820.
- Noether, G. E. (1981). Why Kendall Tau? *Teaching Statistics*, *3*(2), 41–43. <https://doi.org/10.1111/j.1467-9639.1981.tb00422.x>
- Park, R. J., Jacob, D. J., Field, B. D., Yantosca, R. M., & Chin, M. (2004). Natural and transboundary pollution influences on sulfate-nitrate-ammonium aerosols in the United States: Implications for policy. *Journal of Geophysical Research*, *109*, D15204. <https://doi.org/10.1029/2003JD004473>
- Paulot, F., Jacob, D. J., Pinder, R. W., Bash, J. O., Travis, K., & Henze, D. K. (2014). Ammonia emissions in the United States, European Union, and China derived by high-resolution inversion of ammonium wet deposition data: Interpretation with a new agricultural emissions inventory (MASAGE_NH3). *Journal of Geophysical Research: Atmospheres*, *119*, 4343–4364. <https://doi.org/10.1002/2013JD021130>
- Puchalski, M. A., Rogers, C. M., Baumgardner, R., Mishoe, K. P., Price, G., Smith, M. J., et al. (2015). A statistical comparison of active and passive ammonia measurements collected at Clean Air Status and Trends Network (CASTNET) sites. *Environmental Science: Processes & Impacts*, *17*(2), 358–369. <https://doi.org/10.1039/c4em00531g>
- Pye, H. O. T., & Seinfeld, J. H. (2010). A global perspective on aerosol from low-volatility organic compounds. *Atmospheric Chemistry and Physics*, *10*(9), 4377–4401. <https://doi.org/10.5194/acp-10-4377-2010>
- Schiferl, L. D., Heald, C. L., van Damme, M., Clarisse, L., Clerbaux, C., Coheur, P. F., et al. (2016). Interannual variability of ammonia concentrations over the United States: Sources and implications. *Atmospheric Chemistry and Physics*, *16*(18), 12,305–12,328. <https://doi.org/10.5194/acp-16-12305-2016>
- Skjøth, C. A., Hertel, O., Gyldenkaerne, S., & Ellermann, T. (2004). Implementing a dynamical ammonia emission parameterization in the large-scale air pollution model ACDEP. *Journal of Geophysical Research*, *109*, D06306. <https://doi.org/10.1029/2003JD003895>
- Walker, J. M., Philip, S., Martin, R. V., & Seinfeld, J. H. (2012). Simulation of nitrate, sulfate, and ammonium aerosols over the United States. *Atmospheric Chemistry and Physics*, *12*(22), 11,213–11,227. <https://doi.org/10.5194/acp-12-11213-2012>
- Wen, D., Lin, J. C., Zhang, L., Vet, R., & Moran, M. D. (2013). Modeling atmospheric ammonia and ammonium using a stochastic Lagrangian air quality model (STILT-Chem v0.7). *Geoscientific Model Development*, *6*(2), 327–344. <https://doi.org/10.5194/gmd-6-327-2013>
- Yao, X., & Zhang, L. (2016). Trends in atmospheric ammonia at urban, rural, and remote sites across North America. *Atmospheric Chemistry and Physics*, *16*(17), 11,465–11,475. <https://doi.org/10.5194/acp-16-11465-2016>
- Yu, F. (2011). A secondary organic aerosol formation model considering successive oxidation aging and kinetic condensation of organic compounds: Global scale implications. *Atmospheric Chemistry and Physics*, *11*(3), 1083–1099. <https://doi.org/10.5194/acp-11-1083-2011>
- Yu, F., & Luo, G. (2009). Simulation of particle size distribution with a global aerosol model: Contribution of nucleation to aerosol and CCN number concentrations. *Atmospheric Chemistry and Physics*, *9*(20), 7691–7710. <https://doi.org/10.5194/acp-9-7691-2009>
- Yu, F., Nadykto, A. B., Herb, J., Luo, G., Nazarenko, K. M., & Uvarova, L. A. (2018). H₂SO₄-H₂O-NH₃ ternary ion-mediated nucleation (TIMN): Kinetic-based model and comparison with CLOUD measurements. *Atmospheric Chemistry and Physics Discussions*, 1–41. <https://doi.org/10.5194/acp-2018-396>
- Yu, F., Nair, A. A., & Luo, G. (2018). Long-term trend of gaseous ammonia over the United States: Modeling and comparison with observations. *Journal of Geophysical Research: Atmospheres*, *123*, 8315–8325. <https://doi.org/10.1029/2018JD028412>
- Zhang, L., Jacob, D. J., Knipping, E. M., Kumar, N., Munger, J. W., Carouge, C. C., et al. (2012). Nitrogen deposition to the United States: distribution, sources, and processes. *Atmospheric Chemistry and Physics*, *12*(10), 4539–4554. <https://doi.org/10.5194/acp-12-4539-2012>
- Zhu, L., Henze, D., Bash, J., Jeong, G.-R., Cady-Pereira, K., Shephard, M., et al. (2015). Global evaluation of ammonia bidirectional exchange and livestock diurnal variation schemes. *Atmospheric Chemistry and Physics*, *15*(22), 12,823–12,843. <https://doi.org/10.5194/acp-15-12823-2015>
- Zhu, L., Henze, D. K., Cady-Pereira, K. E., Shephard, M. W., Luo, M., Pinder, R. W., et al. (2013). Constraining U.S. ammonia emissions using TES remote sensing observations and the GEOS-Chem adjoint model. *Journal of Geophysical Research: Atmospheres*, *118*, 3355–3368. <https://doi.org/10.1002/jgrd.50166>